Investigation of the critical edge ion heat flux for L-H transitions in Alcator C-Mod and its dependence on B_T

M Schmidtmayr[1], JW Hughes[2], F Ryter[3], E Wolfrum[3], N Cao[2], AJ Creely[2], N Howard[2], AE Hubbard[2], Y Lin[2], ML Reinke[4], JE Rice[2], EA Tolman[2], S Wukitch[2], Y Ma[5], ASDEX Upgrade Team[3], and Alcator C-Mod Team[2]

[1]Institute of Applied Physics, TU Wien, Fusion@ÖAW, Wiedner Hauptstr. 8-10/E134, 1040 Vienna, Austria

[2]Plasma Science and Fusion Center, Massachusetts Institute of Technology, Cambridge, MA, USA

[3]Max-Planck-Institut für Plasmaphysik, Boltzmannstr. 2, D-85748 Garching, Germany

[4]Oak Ridge National Laboratory, Oak Ridge, TN 37831, USA

[5]Fircroft Engineering, Lingley House, 120 Birchwood Point, Birchwood Boulevard, Warrington, WA3 7QH, UK

30 January 2018

Abstract

This paper presents investigations on the role of the edge ion heat flux for transitions from L-mode to H-mode in Alcator C-Mod. Previous results from the ASDEX Upgrade tokamak indicated that a critical value of edge ion heat flux per particle is needed for the transition. Analysis of C-Mod data confirms this result. The edge ion heat flux is indeed found to increase linearly with density at given magnetic field and plasma current. Furthermore, the Alcator C-Mod data indicate that the edge ion heat flux at the L-H transition also increases with magnetic field. Combining the data from Alcator

C-Mod and ASDEX Upgrade yields a general expression for the edge ion heat flux at the L-H transition. These results are discussed from the point of view of the possible physics mechanism of the L-H transition. They are also compared to the L-H power threshold scaling and an extrapolation for ITER is given.

1 Introduction

The H-mode is a plasma regime with improved particle and energy confinement induced by a transport barrier at the plasma edge where turbulent transport is suppressed. The H-mode is usually accessed from the L-mode across the L-H transition by surpassing a certain heating power threshold, P_{LH}, which depends on several factors and experimental conditions. In particular, it increases with magnetic field while the density dependence exhibits a non-monotonic behaviour with a distinct minimum, labelled here $\bar{n}_{e,min}$, which separates the so-called low and high density branches. The density behavior has been studied on several tokamaks, including Alcator C-Mod [1], ASDEX Upgrade [2], JET [3, 4] and DIII-D [5].

Multi-machine studies made over the last two decades have yielded empirical scaling expressions for the power threshold. The most recent of them [6], valid only in the high density branch, reads:

$$P_{LH,scal} = 0.049 \bar{n}_e^{0.72} B_T^{0.8} S^{0.94} \tag{1}$$

where B_T is the toroidal magnetic field in T, $\bar{n}_e$ the line averaged density in $10^{20} m^{-3}$ and S the plasma surface area in m^2, yielding $P_{LH,scal}$ in MW. This expression is only valid for magnetic configurations with the ion ∇B drift directed towards the X-point, commonly known as 'favorable'.

It is widely accepted that the improved confinement is a result of sheared $E \times B$ flows at the plasma edge, which suppress turbulent transport and lead to the formation

of the transport barrier [7, 8, 9, 10]. The ExB flows are mainly induced by a well in the radial electric field, E_r, at the very edge of the plasma, whereby the neo-classical contribution driven by the main plasma ions [11, 12] likely plays a main role. Equation (4) of Reference [13] simplifies to an expression for E_r that is the sum of a term proportional to the parallel flow and a main ion diamagnetic term $\nabla p_i/(n_i e)$, where p_i is the main ion pressure, n_i the main ion density and e the elementary charge. Neglecting parallel flows, the neo-classical radial electric field can be approximated as $E_r \approx \nabla p_i/(n_i e)$. For flat density profiles, this simplifies to $E_r \propto \nabla T_i$, where T_i is the ion temperature. Experimental data in the edge of established H-modes support this approximation, when applied to the main ion species, despite its being inappropriate to the medium-Z impurities typically used to measure E_r by charge exchange spectroscopy [12, 14]. Even if a finite amount of parallel flow is present, the gradient in E_r will be dominated by the ion pressure term, provided the flow term is radially uniform. This assumption is valid for discharges with no external torque from neutral beam injection. In L-mode, the E_r well at the plasma edge may deepen when p_i increases, such that ∇E_r increases in magnitude and the shearing rate too, leading eventually to turbulence suppression. Based on these considerations, one may speculate that the ion heat flux at the plasma edge impacts ∇E_r through ∇p_i and can induce the turbulence reduction at a certain value.

This hypothesis has been investigated experimentally in the ASDEX Upgrade tokamak. Evidence was shown that critical values of edge T_i and E_r well depth occur at the L-H transition, in a range of density spanning the low and high density branch [15]. Subsequently this was linked to the degree of ion heat flux at the plasma edge, $q^{LH}_{i,edge}$ [16, 17]. The ion heat flux is calculated by power balance analysis, which is only possible in cases in which the electron and ion heat channels can be separated. In practice this turned out to be the case in the low density branch. In contrast to the non-monotonic dependence of P_{LH} on density, $q^{LH}_{i,edge}$ exhibits a linear increase with density, consistent with the assumption that a sufficiently deep E_r well is required at the L-H transition. The different behaviour of P_{LH} and $q^{LH}_{i,edge}$ is attributed to the

fact that towards low density the contribution of the electron-ion collisional energy exchange becomes weaker, such that a high heating power is needed to achieve the required ion heat flux value. This, of course, depends on the fraction of direct electron and ion heating provided by the auxiliary heating method that is used to reach the H-mode. When comparing the trends at low density of P_{LH} and the surface integrated ion heat flux $Q^{LH}_{i,edge}$, one finds that the deviation is smaller when the proportion of direct ion heating is high [17].

A complementary body of theoretical and experimental work has recently highlighted interesting dynamics in the interaction of edge turbulence and mean flows in the vicinity of L-H transitions. (See [18] and references therein.) Transfer of energy from turbulent fluctuations to large scale zonal flow (ZF) can occur in the period prior to an L-H transition, when sufficient $E \times B$ flow shear is attained to suppress fully fluctuations over long time scales. This transfer of turbulent energy into ZF can lead to observed limit cycle oscillations, and provides a potential trigger mechanism for the final L-H transport bifurcation. However, for H-mode sustainment, a sufficient ∇T_i must be present to support the E_r well, and thus the macroscopic model discussed in this article remains compatible with the turbulence/ZF mechanism for L-H dynamics and transition trigger. Indeed, effort to link the two mechanisms via numerical modeling [19] supports the primary role of edge ion pressure gradient in establishing mean flow shear, and reinforces the hypothesis that reduced electron-ion coupling is to blame for the elevated H-mode power threshold in the low density branch.

The L-H transition power threshold has been extensively studied in the Alcator C-Mod tokamak [1, 20, 21, 22, 23, 24, 25]. In particular the non-monotonic density dependence is clearly observed. These studies provide a wide set of discharges to investigate the possible role of the edge ion heat flux in the L-H transition, in a similar way as done for ASDEX Upgrade (AUG) and this is the subject of the present work. C-Mod provides an opportunity to test the hypothesis that a critical edge ion heat flux determines H-mode access, in a distinct parameter range. The main quantities having a strong impact on P_{LH} are quite different from those in ASDEX Upgrade: magnetic

field and plasma density are much higher while plasma surface area is much smaller.

The paper is structured as follows: Section 2 describes the experimental setup and data preparation, the results for the edge ion heat flux are presented in Section 3 and in Section 4 they are summarized and discussed.

2 Experimental setup and analysis method

2.1 Experiments and diagnostics

Alcator C-Mod [26, 27, 28] is a high field compact tokamak with major radius $R = 0.68$m and minor radius $a = 0.22$m, and a plasma surface area S of approximately 7m^2. The magnetic field values of the C-Mod discharges used in this work were mostly around 5.4T, with a smaller set of discharges available at 4.0T and 7.8T. The plasma current was $0.9MA$ in all the discharges. By comparison, in ASDEX Upgrade (AUG) $R = 1.65$m, $a = 0.5$m and $S \approx 44\text{m}^2$ and the ion heat flux analysis was carried out at a single magnetic field value of 2.35T. On C-Mod the auxiliary heating method was ion cyclotron heating (ICH). For the 5.4T discharges, the ICH frequency was 80MHz, giving first harmonic absorption on the H minority species at $r/a \approx 0$. For 4.0T discharges, ICH at 70MHz was used, damping again on H, but off-axis at $r/a \approx 0.5$. In 7.8T discharges, ICH at 80MHz absorbs on an injected ^3He minority. In the D(H) heating schemes at $B_T < 6$T, the fraction of electron heating is high, while in the ^3He scenario at $B_T > 7$T, the balance of the heating is shifted more toward the ions.

Power balance analysis requires kinetic profiles which were provided by the following diagnostics. The electron density n_e was measured with a Thomson Scattering (TS) diagnostic [29]. The TS has a spatial resolution of 1-2cm in the core and 1-2mm at the plasma edge, when mapped to the machine midplane. The electron temperature T_e was measured with the TS, as well as with electron cyclotron emission (ECE) measured with multichannel grating polychromators in the second harmonic extraordinary mode emission [30]. The TS and ECE data were then combined to create a single polynomial

fit. The ion temperature profiles were deduced from X-ray imaging crystal spectroscopy (XICS) [31]. XICS measures the line-radiation emitted by helium-like and hydrogen-like argon ions, introduced earlier in the discharge by an argon puff. The measured spectra are inverted to ion temperature profiles with the software package THACO [31]. Significant signals from these Ar charge states are obtained mainly in the core plasma, where T_e increases, which means that XICS can provide useful T_i profiles in the interior, up to $r/a \approx 0.80$. Ar puffs are not applied universally to C-Mod discharges, and are usually kept small to avoid undesirable levels of core radiated power. As a result XICS data at low density are subject to low signal-to-noise ratios, and the uncertainty in T_i tends to dominate over other instrumental sources. Core radiated power was measured by gold foil bolometers [30]. The magnetic equilibrium was calculated by EFIT [32].

The C-Mod discharges presented here were carried out in deuterium plasmas for dedicated L-H threshold studies during the 2011, 2014, 2015 and 2016 campaigns, extending the work presented in [1, 24]. The ICH power was either increased in small steps or ramped up continuously for an accurate determination of the LH power threshold. All the discharges have been performed in the lower single null configuration with the ion ∇B drift directed towards the X-point, *i.e.* in the usual favorable configuration for H-mode access. As reported previously, the L-H power threshold in C-Mod depends on the magnetic configuration, P_{LH} being reduced when the outer strike point is moved from the conventional location on the vertical plate divertor to the floor of the divertor slot [24, 33]. In the present work we analyze only discharges in the vertical target configuration because the necessary T_i data are not available for the slot configuration. Prior results [33] indicate that the difference in P_{LH} between the slot and divertor configurations is small when operating near or in the low density branch, which is where the analysis in this paper concentrates.

The density range in which the separation of the electron and ion channels can be observed using power balance analysis (see Section 2.2) is $0.9 \cdot 10^{20} m^{-3} \leq \bar{n}_e \leq 1.5 \cdot 10^{20} m^{-3}$, which places these discharges near or in the low density branch for H-mode access, as on ASDEX Upgrade. The power threshold is, as is usually done

in such studies, calculated from P_{loss} taken just before the L-H transition: $P_{LH} = P_{heat} - dW/dt$ where P_{heat} is here $P_{OH} + P_{ICH}$, with ohmic power P_{OH}, absorbed ICH heating power P_{ICH}, and W is the plasma stored energy.

Figure 1 shows selected quantities for a typical discharge in our L-H transition study. The auxiliary ICH power (purple) is increased continuously from 0.5 to 2.0 MW. Around 1.14s the plasma transitions into H-mode, then transitions back into L-mode at 1.4s after the ICH is turned off. The LH-transition is typically indicated by a sharp drop in the Dα signal, which is clearly visible in the bottom box in Figure 1. After 1.14s, the density and temperature traces show a strong increase due to the formation of the edge pedestals.

2.2 The power balance analysis

Ion heat flux is obtained by a time-dependent power balance analysis performed with the TRANSP code [34]. To determine the ICH deposition in the electron and ion channels TRANSP utilizes the full-wave TORIC code [35]. The global RF absorption must be imposed and was set to 85% for the D(H) scheme at 5.4T, based on prior experimental determination [36]. For the off-axis heating condition at 4.0T, we assume a reduced overall absorption of 75%. We take 40% for the ^3He cases at 7.8T, following the investigations reported in [25]. The acquisition of density and temperature profiles used as inputs for TRANSP was described in the previous subsection. The electron-ion collisional energy exchange, p_{ie}, can be an important component in this analysis, and the electron and ion heat channel can only be separated if this term is small or well defined, the latter meaning that the difference between T_e and T_i is larger than the experimental uncertainties. As indicated in [17], this limited the analysis in ASDEX Upgrade to the low density branch, which is also the case here.

Due to diagnostics issues, some constraints had to be imposed on the TRANSP calculations. The spectroscopic measurement of the hydrogen concentration is noisy and a fixed value of 5% was used for all calculations. This value is usual for C-Mod

plasmas and a sensitivity scan has been performed to assess its impact on $q_{i,edge}$, as presented below. An additional sensitivity study was done for the ^3He concentration in the higher field case. These sensitivity scans are discussed in Section 2.3.

XICS does not provide reliable T_i data outside of $\rho_{tor} \approx 0.80$, where ρ_{tor} is the normalized toroidal flux coordinate used in TRANSP. However we can take advantage of the strong electron-ion coupling in the outer region of C-Mod plasmas and constrain the T_i profile to match T_e for $\rho_{tor} \geq \rho_{ei}$, where we specify the location at which ions and electrons are equilibrated: ρ_{ei}. The assumption of $T_e = T_i$ was verified in some plasmas for which T_e from TS were compared to T_i from charge exchange (CXRS) data. In the 5.4T discharges analyszed here, ρ_{ei} is set to 0.9. Because of reduced XICS data quality in the lower and higher field discharges, the 4.0T cases assumed $\rho_{ei} = 0.6$ and the 7.8T case assumed $\rho_{ei} = 0.85$. Heat transfer from electrons to ions p_{ie} will be zero for $\rho_{tor} > \rho_{ei}$, and generally finite for $\rho_{tor} < \rho_{ei}$

The Z_{eff} measurements in C-Mod are usually not very noisy but suffer from systematic uncertainties. Therefore, Z_{eff} for each discharge was set to a constant value in time which was close to the measured Z_{eff} just before the L-H transition of each discharge. This constraint affects the electron heat flux but not the ion heat flux calculations.

2.3 Error estimation and sensitivity studies

To establish the error bars presented in the plots in the following sections, several sensitivity studies were performed which are presented in this subsection. The minority concentration has a crucial impact on the absorbed ICH power, and was set to 5% as mentioned above. This is a reasonable value for C-Mod, but deviations from it are possible. In a series of TRANSP runs for discharge 1140801032, the minority concentration was increased from 1% to 10% in 1% increments. Figure 2a shows the resulting impact of this variation on Q_i, which increases or decreases by not more than 6%. A similar though less comprehensive study was performed for 1160713011 to

investigate the impact of the He^3 minority concentration, which was increased from 3% to 10% and resulted in less than 3% deviation from Q_i with the initial 5% concentration (seen in Figure 2b).

Variations of the ion temperature, while keeping T_e fixed, have a far larger impact. For this part of the study, the entire ion temperature profile was multiplied by a constant factor, increasing or decreasing the ion temperature by 10%. As expected, this had a major impact on the ion heat flux through the collisional energy exchange term. Decreasing the ion temperature leads to more power flowing from the electron channel to the ion channel and therefore a higher Q_i. Figure 3 shows that Q_i increases or decreases by up to 13% making the ion temperature, or more generally the difference between the electron and ion temperatures, a significant error source.

In section 2.2, the constraint was introduced that, outside of a certain ρ_{ei}, T_i is equal to T_e. This constraint has a significant impact on the edge ion heat flux because it sets $p_{ei} = 0$ outside of ρ_{ei}. This is illustrated by Figure 4. The lefthand plot shows the T_i fit to XICS data being constrained to match T_e using several choices for ρ_{ei}. The influence this constraint has on Q_i values calculated for this discharge (shot 1160713011) is shown at right. If ρ_{ei} decreases from 0.9 to 0.6, the ion heat flux drops by 33%. Summarizing, the most important source of uncertainties is caused by those on the temperature profiles, in particular Ti. These are taken into account in the error bars indicated in the plots of the following sections.

3 The edge ion heat flux at the L-H transition

3.1 Density dependence at 5.4T

The ion channel as calculated in the power balance for these experiments consists of two contributions: the heat deposited in the ion heat channel by the minority ions accelerated by the ICH and the electron-ion heat exchange p_{ie}. In general T_e is larger than T_i over a major part of the radius such that p_{ie} contributes positively to the ion

heat channel. In the following we use the surfaced-integrated quantities, in particular for the ion heat flux because this quantity can be directly compared to the threshold power. An example of the analysis is illustrated in figure 5 which shows the profiles of the surface integrated heat flux due to absorption by ions from ICH ($Q_{i,ICH}$), the surface integrated heat flux due to heat transfer from electrons to ions (Q_{ie}), and the resulting profile of the surface-integrated total ion heat flux (Q_i). These profiles are shown for two discharges, one with rather low density and one from the high density region of the data set. Figure 5 demonstrates the importance of the heat exchange term Q_{ie}. While ICH and heat exchange contribute each about half of the entire ion heat flux in the low density case, Q_{ie} becomes a dominant part at higher densities. Q_{ie} is constant in radius outside of $\rho_{tor} = 0.9$, where $T_e = T_i$ is enforced, as discussed in section 2.2.

We analyzed several discharges with $B_T = 5.4T$ and $I_P = 0.9MA$ at different densities, computing power balance from TRANSP in the L-mode phase immediately prior to the H-mode formation. The quantities shown below were calculated from TRANSP time-series data using a causal moving time average with a window of 20ms. Figure 6 shows the surface integrated ion heat flux $Q_{i,edge}$ at $\rho_{tor} = 0.98$ as well as P_{LH} versus density. Despite the scatter in $Q_{i,edge}$ the result exhibits a linear increase with the line-averaged density which is similar to the ASDEX Upgrade results, [17]. A linear free fit to this dataset crosses the X-axis at $n_e = 0.1 \cdot 10^{19}\mathrm{m}^{-3}$, which is very close to the origin. We therefore elect to force a linear fit through the origin, shown as the solid line in Figure 6. The resultant scaling is $Q_{i,edge}^{LH,fit} = 0.065\bar{n}_e$ with $Q_{i,edge}^{LH,fit}$ in MW and $\bar{n}_e$ in $10^{19}\mathrm{m}^{-3}$. This expression will be compared quantitatively to the ASDEX Upgrade results in the next section.

Figure 6 compares the surface integrated ion heat flux directly to the total power at threshold, also calculated by TRANSP. The TRANSP values for P_{LH} are higher than the dashed curve, which was previously obtained by fitting to threshold power data from a separate set of discharges in [1], and which shows the nominal transition point between the low density and high density branches of P_{LH} ($\bar{n}_{e,min} \approx 1.3 \cdot 10^{20}\mathrm{m}^{-3}$).

For the present set of discharges, we find that the conventional calculation of P_{OH} from the time-dependent EFIT magnetic equilibrium is systematically smaller than the Ohmic power calculated in TRANSP on the basis of the T_e, n_e, Z_{eff} profiles and the neoclassical resistivity. This discrepancy introduces uncertainty in the value of total P_{LH}, of which P_{OH} is a significant fraction. However, this uncertainty is not significant to the key results of this paper, because it only effects the electron heating term and not the ion heat flux analysis.

3.2 Comparison with ASDEX Upgrade

In both AUG and C-Mod the surface-integrated edge ion heat flux at the L-H transition increases with density. As mentioned above, we used the surface-integrated flux for comparison with P_{LH}, but the actual physics quantity which determines ∇T_i and therefore the E_r well through ∇p_i is $q_i = Q_i/S$, the heat flux in Wm^{-2}. This explains the plasma surface dependence ($S^{0.94}$) in the P_{LH} scaling [6] and indicates that the appropriate quantity for comparisons between devices is q_i and not Q_i. The corresponding expressions for AUG and C-Mod, with $S_{AUG} \approx 44m^2$ and $S_{CMOD} \approx 7m^2$, are then:

$$q_{i,edge}^{LH,AUG} = 0.0041\bar{n}_e$$

$$q_{i,edge}^{LH,CMOD} = 0.0093\bar{n}_e$$

with $\bar{n}_e$ in $10^{19}m^{-3}$ and $q_{i,edge}$ in MWm^{-2}.

The power threshold scaling law exhibits a toroidal magnetic field dependence. Assuming that a critical $E \times B$ velocity shearing is required at the L-H transition, with $\left|\frac{\vec{E}\times\vec{B}}{B^2}\right|_{crit} \sim \frac{E_{r,crit}}{B} \sim \frac{\nabla p_{i,crit}}{B}$ one may speculate that the critical $q_{i,edge}^{LH}$, which impacts directly on ∇p_i might exhibit a linear magnetic field dependence to compensate for B in the denominator. Under this assumption, we can further compare the two above

expressions by using the slope from AUG to predict a slope for C-Mod:

$$0.0041\frac{B_{T,C-Mod}}{B_{T,AUG}} = 0.0094 \tag{2}$$

with $B_{T,C-Mod} = 5.4T$ and $B_{T,AUG} = 2.35T$. The predicted slope agrees surprisingly well with the slope calculated from the C-Mod data. This motivated us to investigate the B_T dependence which can be deduced from the C-Mod data, as described in the following section.

3.3 B_T dependence of the edge ion heat flux

The B_T dependence of $Q_{i,edge}^{LH}$ has been tentatively investigated by also analyzing discharges at 7.8T and 4T, therefore respectively above and below the 5.4T cases presented in the first part of this section. Unfortunately the number of discharges providing the required data and experimental conditions to investigate this aspect are rare: only one discharge at 7.8T and two at 4T can be presented here. The results are shown in Figure 7, together with the 5.4T cases presented above.

As in the 5.4T cases, the two 4.0T cases used ICH heating on the hydrogen minority, but at the lower field, power deposition was strongly off-axis on the high field side. The ICH power is deposited around $R = 0.54$m, or $r/a \approx 0.65$. The plasma volume where the power is deposited is larger than for a deposition closer to the center which leads to a lower energy of the minority hydrogen tail and thus a somewhat higher fraction of direct ion heating. TRANSP calculations indicating the increased ratio of heating power to ions are illustrated in Figure 8. The overall ICH absorption in these 4.0T cases is estimated to be at most 75%. The $Q_{i,edge}^{LH}$ values for the 4T cases shown in Figure 7 are not demonstrably lower than the 5.4T cases, and the total P_{LH} inferred is actually larger than at 5.4T. This would appear at variance with the expectation that both P_{LH} and $Q_{i,edge}^{LH}$ should increase with B_T. However, if we consider that the assumed absorption efficiency of ICH is an upper bound, then the values of P_{LH} and $Q_{i,edge}^{LH}$ could also be considerably lower in the 4.0T cases. Note that this is consistent

with the relatively weak scaling of P_{LH} with B_T reported on C-Mod in [1].

At 7.8T, ICH heating is done at 80MHz on a ^{3}He minority species. Here an improved estimate of the total ICH absorption is available from a break-in-slope analysis of the plasma stored energy in response to RF power cut-offs [25]. Based on this analysis, we deduce a lower bound of 40% for ICH absorption in 7.8T L-modes, and specify this number as an input to the TRANSP analysis. The fraction of ICH power delivered to ions *vs.* electrons is quite high in the D(^{3}He) heating scheme, as indicated in Figure 8. The sensitivity study presented in section 2.3 indicates that the minority concentration only weakly impacts $Q^{LH}_{i,edge}$.

Figure 7 shows that the calculated $Q^{LH}_{i,edge}$ for 7.8T is notably higher than at 5.4T. Because the assumption of 40% ICH absorption was conservative, the actual value of ion heat flux could be yet higher in the 7.8T case. This supports the assumption of a positive B_T dependence of the critical edge ion heat flux for the L-H transition. As a result of the much higher ion heating fraction at 7.8T with D(^{3}He) ICH, the total P_{LH} is very similar to that obtained at 5.4T with D(H) ICH.

Taken altogether these results illustrate the importance of quantitative estimation of total heating, as well as the ratio of ion to electron heating, when attempting to scale power threshold across operational spaces on a given machine. The effect of the fraction of ion to electron heating on C-Mod is similar to the AUG results obtained in comparisons between electron cyclotron heating and neutral beam injection, the latter yielding a significantly higher ion heating [17].

Summarizing, the 7.8T case clearly indicates a positive B_T dependence of $q^{LH}_{i,edge}$. Considering the experimental uncertainties, the 4T cases do not contradict this result, however they do not contribute quantitatively. This first observation of a B_T influence on $q^{LH}_{i,edge}$ from a single machine, together with the cross-machine trends discussed in Section 3.2, provide evidence for the key role played by the ion heat flux in the L-H transition.

4 Joint machine analysis and outlook for ITER

Despite significant differences in machine parameters (size, magnetic field, density) between AUG and C-Mod, evidence on both machines shows that a critical edge ion heat flux is needed for access to H-mode, and that this critical $q_{i,edge}^{LH}$ scales linearly with density on either machine. Equipped with the results from this C-Mod study, as well as the data from prior AUG work [17], we can explore whether the two devices in combination can produce a common expression for $q_{i,edge}^{LH}$. For this purpose we performed a regression on the $q_{i,edge}^{LH}$ data of the two devices to deduce the density and B_T dependences. The resulting expression, in the usual power law form, reads:

$$q_{i,fit}^{LH} = 0.0021 \bar{n}_e^{1.07 \pm 0.09} B_T^{0.76 \pm 0.2} \tag{3}$$

with $\bar{n}_e$ in $10^{19} m^{-3}$ and B_T in tesla, yielding $q_{i,edge}^{LH}$ in MWm^{-2}, with an RMSE of 0.18.

This expression exhibits the linear density dependence found individually in each device and, as expected, a positive B_T dependence which is close to that of P_{LH}. The uncertainties in the exponents, which correspond to one standard deviation, indicate that the density dependence is well characterized while that of the magnetic field suffers from the small number of points at 4T and 7.8T. The effectiveness of the scaling is illustrated in figure 9 which shows the experimental $q_{i,edge}^{LH}$ values as a function of the scaling expression prediction: within the respective error bars, the data points are well aligned. The RMSE drops down to 0.14 and the uncertainties on the exponents are reduced if the outlier low-power point at 5.4T is not included in the regression, whereas the exponents themselves almost do not change. However, no physics or experimental reason was found to omit this point.

It is underlined that Equation (3) does not include any size scaling, since the surface area dependence effectively is taken into account by using q_i. We verified that including the machine size in the regression yields a size dependence which is close to zero.

In contrast, applying the regression to the surface-integrated ion heat flux, $Q^{LH}_{i,edge}$, yields very similar $\bar{n}_e$ and B_T dependences as in Equation (3), but in addition a $S^{0.93}$ dependence:

$$Q^{LH}_{i,fit} = 0.0029 \bar{n}_e^{1.05\pm0.1} B_T^{0.68\pm0.3} S^{0.93\pm0.2} \tag{4}$$

with RMSE = 0.18. In this expression the density dependence is stronger than in the ITPA P_{LH} scaling law of Equation (1), but both the B_T and S dependences are in good agreement. Despite the fact that the additional variable S has been included in the regression, the RMSE does not decrease relative to Eq. (3), from which we conclude that q_i is indeed the right physics quantity. However, Eq. (4) may be useful for comparisons with P_{LH} or for practical experimental cases.

Applying Eq. (4) to ITER at $\bar{n}_e = 5 \cdot 10^{19} m^{-3}$ yields about 20 MW for Q_i which is perfectly compatible with the 52MW predicted according to Eq. (1) for P_{LH}. We offer that the expression for the critical ion heat flux we provide in this paper may be useful for comparisons to the transport and confinement modeling studies which are presently being carried out for ITER.

5 Summary and Conclusion

Following the work carried out in ASDEX Upgrade [17], the edge ion heat flux at the L-H transition, $q^{LH}_{i,edge}$, has been studied in Alcator C-Mod. To guarantee the separation between the electron and ion heat channels, the required power balance analysis can only be performed near or in the low density branch of the power threshold. In both devices $q^{LH}_{i,edge}$ below a critical density ($\bar{n}_e < 1.3 \cdot 10^{20}\mathrm{m}^{-3}$ for C-Mod, $\bar{n}_e < 0.4 \cdot 10^{20}\mathrm{m}^{-3}$ for AUG) is found to increase linearly with density whereas the power threshold P_{LH} decreases. These different density dependences between these two quantities are explained by the contribution of the electron-ion energy exchange to the ion heat flux.

In addition to the density dependence, the magnetic field dependence of $q^{LH}_{i,edge}$

could also be addressed in C-Mod. The results are consistent with an increase of the ion heat flux with magnetic field strength, in agreement with physics assumptions on the role of the velocity shearing by the neoclassical radial electric field in the reduction of turbulent transport at the L-H transition and consistent with the B_T dependence of the power threshold.

As C-Mod and AUG are very different in size, magnetic field and density, combining the data sets from the two devices provides a significant extension of the study carried out in AUG. A joint analysis of data from the two devices determines a scaling for the critical edge ion heat flux which scales nearly linearly with both density and magnetic field. By implication, a critical ion heat flux per particle is needed to allow access to the L-H transition, and this critical value scales with field. This is consistent with a paradigm of the L-H transition occuring when a critical value of edge $E \times B$ shear $\sim E_r/B$ is approached. Applying the derived scaling law to ITER projects a required surface-integrated ion heat flux that is just less than half the total power threshold projected by the ITPA P_{LH} scaling law.

Acknowledgments

The authors wish to thank Professor F. Aumayr for his support. M. Schmidtmayr is a fellow of the Austrian Marshall Plan Foundation, which provided support for this work. This work has been partly carried out within the framework of the EUROfusion Consortium and has received funding from the Euratom research and training program 2014-2018 under grant agreement No 633053. The views and opinions expressed herein do not necessarily reflect those of the European Commission. Further support came from U.S. Department of Energy awards DE-FC02-99ER54512, DE-SC0014264 using Alcator C-Mod, a DOE Office of Science User Facility.

References

[1] Y Ma, JW Hughes, AE Hubbard, B LaBombard, RM Churchill, T Golfinopolous, N Tsujii, and ES Marmar. Scaling of h-mode threshold power and l–h edge conditions with favourable ion grad-b drift in alcator c-mod tokamak. *Nuclear Fusion*, 52(2):023010, 2012.

[2] F Ryter, T Pütterich, M Reich, A Scarabosio, E Wolfrum, R Fischer, M Gemisic Adamov, N Hicks, B Kurzan, C Maggi, et al. H-mode threshold and confinement in helium and deuterium in asdex upgrade. *Nuclear Fusion*, 49(6):062003, 2009.

[3] Y Andrew, R Sartori, E Righi, E De la Luna, S Hacquin, DF Howell, NC Hawkes, LD Horton, A Huber, A Korotkov, et al. H-mode access in the low density regime on jet. *Plasma Physics and Controlled Fusion*, 48(4):479, 2006.

[4] Costanza F Maggi, E Delabie, Theodore M Biewer, M Groth, NC Hawkes, M Lehnen, E de la Luna, K McCormick, C Reux, F Rimini, et al. L–h power threshold studies in jet with be/w and c wall. *Nuclear Fusion*, 54(2):023007, 2014.

[5] P Gohil, TE Evans, ME Fenstermacher, JR Ferron, TH Osborne, JM Park, O Schmitz, JT Scoville, and EA Unterberg. L–h transition studies on diii-d to determine h-mode access for operational scenarios in iter. *Nuclear Fusion*, 51(10):103020, 2011.

[6] YR Martin, T Takizuka, et al. Power requirement for accessing the h-mode in iter. In *Journal of Physics: Conference Series*, volume 123, page 012033. IOP Publishing, 2008.

[7] R. J. Taylor, M. L. Brown, B. D. Fried, H. Grote, J. R. Liberati, G. J. Morales, P. Pribyl, D. Darrow, and M. Ono. H. *Phys. Rev. Lett.*, 63:2365–2368, Nov 1989.

[8] H Biglari, PH Diamond, and PW Terry. Influence of sheared poloidal rotation on edge turbulence. *Physics of Fluids B: Plasma Physics*, 2(1):1–4, 1990.

[9] RJ Groebner. An emerging understanding of h-mode discharges in tokamaks. *Physics of Fluids B: Plasma Physics*, 5(7):2343–2354, 1993.

[10] KH Burrell. Effects of exb velocity shear and magnetic shear on turbulence and transport in magnetic confinement devices. *Physics of Plasmas*, 4(5):1499–1518, 1997.

[11] FL Hinton and RD Hazeltine. Theory of plasma transport in toroidal confinement systems. *Reviews of Modern Physics*, 48(2):239, 1976.

[12] E Viezzer, T Pütterich, GD Conway, R Dux, T Happel, JC Fuchs, RM McDermott, F Ryter, B Sieglin, W Suttrop, et al. High-accuracy characterization of the edge radial electric field at asdex upgrade. *Nuclear Fusion*, 53(5):053005, 2013.

[13] Ulrich Stroth, P Manz, and M Ramisch. On the interaction of turbulence and flows in toroidal plasmas. *Plasma Physics and Controlled Fusion*, 53(2):024006, 2011.

[14] RM McDermott, B Lipschultz, JW Hughes, PJ Catto, AE Hubbard, IH Hutchinson, RS Granetz, M Greenwald, B LaBombard, K Marr, et al. Edge radial electric field structure and its connections to h-mode confinement in alcator c-mod plasmas a. *Physics of Plasmas*, 16(5):056103, 2009.

[15] P. Sauter, T. Puetterich, F. Ryter, E. Viezzer, E. Wolfrum, G.D. Conway, R. Fischer, B. Kurzan, R.M. McDermott, S.K. Rathgeber, and the ASDEX Upgrade Team. L- to h-mode transitions at low density in asdex upgrade. *Nuclear Fusion*, 52(1):012001, 2012.

[16] F Ryter, SK Rathgeber, L Barrera Orte, M Bernert, GD Conway, R Fischer, T Happel, B Kurzan, RM McDermott, A Scarabosio, et al. Survey of the h-mode power threshold and transition physics studies in asdex upgrade. *Nuclear Fusion*, 53(11):113003, 2013.

[17] F Ryter, L Barrera Orte, B Kurzan, RM McDermott, G Tardini, E Viezzer, M Bernert, R Fischer, et al. Experimental evidence for the key role of the ion heat channel in the physics of the l–h transition. *Nuclear Fusion*, 54(8):083003, 2014.

[18] G R Tynan, I Cziegler, P H Diamond, M Malkov, A Hubbard, J W Hughes, J L Terry, and J H Irby. Recent progress towards a physics-based understanding of the h-mode transition. *Plasma Physics and Controlled Fusion*, 58(4):044003, 2016.

[19] M. A. Malkov, P. H. Diamond, K. Miki, J. E. Rice, and G. R. Tynan. Linking the micro and macro: L-h transition dynamics and threshold physics. *Physics of Plasmas*, 22(3):032506, 2015.

[20] JA Snipes, RS Granetz, M Greenwald, IH Hutchinson, D Garnier, JA Goetz, SN Golovato, A Hubbard, JH Irby, B LaBombard, et al. First ohmic h modes in alcator c-mod. *Nuclear fusion*, 34(7):1039, 1994.

[21] JA Snipes, AE Hubbard, DT Garnier, SN Golovato, RS Granetz, M Greenwald, IH Hutchinson, J Irby, B LaBombard, ES Marmar, et al. H-modes on alcator c-mod. *Plasma Physics and Controlled Fusion*, 38(8):1127, 1996.

[22] JA Snipes, RS Granetz, M Greenwald, OJWF Kardaun, A Kus, F Ryter, U Stroth, J Kollermeyer, SJ Fielding, M Valovic, et al. H mode power threshold database for iter. *Nuclear Fusion*, 36(9):1217, 1996.

[23] Brian LaBombard, JE Rice, AE Hubbard, JW Hughes, M Greenwald, RS Granetz, JH Irby, Y Lin, B Lipschultz, ES Marmar, et al. Transport-driven scrape-off layer flows and the x-point dependence of the l-h power threshold in alcator c-mod a. *Physics of Plasmas*, 12(5):056111, 2005.

[24] Y Ma, JW Hughes, AE Hubbard, B LaBombard, and J Terry. H-mode power threshold reduction in a slot-divertor configuration on the alcator c-mod tokamak. *Plasma physics and controlled fusion*, 54(8):082002, 2012.

[25] EA Tolman, JW Hughes, SM Wolfe, SJ Wukitch, B LaBombard, Hubbard AE, ES Marmar, PB Snyder, and M Schmidtmayr. Influence of high magnetic field on access to stationary h-modes and pedestal characteristics in alcator c-mod. *Nuclear Fusion*, 2018, accepted.

[26] I. H. Hutchinson, R. Boivin, F. Bombarda, P. Bonoli, S. Fairfax, C. Fiore, J. Goetz, S. Golovato, R. Granetz, M. Greenwald, S. Horne, A. Hubbard, J. Irby, B. LaBom-

bard, B. Lipschultz, E. Marmar, G. McCracken, M. Porkolab, J. Rice, J. Snipes, Y. Takase, J. Terry, S. Wolfe, C. Christensen, D. Garnier, M. Graf, T. Hsu, T. Luke, M. May, A. Niemczewski, G. Tinios, J. Schachter, and J. Urbahn. First results from alcator c-mod. *Physics of Plasmas*, 1(5):1511–1518, 1994.

[27] E. S. Marmar and Alcator C-Mod Group. The alcator c-mod program. *Fusion Science and Technology*, 51:261–265, 2007.

[28] M. Greenwald, A. Bader, S. Baek, M. Bakhtiari, H. Barnard, W. Beck, W. Bergerson, I. Bespamyatnov, P. Bonoli, D. Brower, D. Brunner, W. Burke, J. Candy, M. Churchill, I. Cziegler, A. Diallo, A. Dominguez, B. Duval, E. Edlund, P. Ennever, D. Ernst, I. Faust, C. Fiore, T. Fredian, O. Garcia, C. Gao, J. Goetz, T. Golfinopoulos, R. Granetz, O. Grulke, Z. Hartwig, S. Horne, N. Howard, A. Hubbard, J. Hughes, I. Hutchinson, J. Irby, V. Izzo, C. Kessel, B. LaBombard, C. Lau, C. Li, Y. Lin, B. Lipschultz, A. Loarte, E. Marmar, A. Mazurenko, G. McCracken, R. McDermott, O. Meneghini, D. Mikkelsen, D. Mossessian, R. Mumgaard, J. Myra, E. Nelson-Melby, R. Ochoukov, G. Olynyk, R. Parker, S. Pitcher, Y. Podpaly, M. Porkolab, M. Reinke, J. Rice, W. Rowan, A. Schmidt, S. Scott, S. Shiraiwa, J. Sierchio, N. Smick, J. A. Snipes, P. Snyder, B. Sorbom, J. Stillerman, C. Sung, Y. Takase, V. Tang, J. Terry, D. Terry, C. Theiler, A. Tronchin-James, N. Tsujii, R. Vieira, J. Walk, G. Wallace, A. White, D. Whyte, J. Wilson, S. Wolfe, G. Wright, J. Wright, S. Wukitch, and S. Zweben. 20 years of research on the alcator c-mod tokamak. *Physics of Plasmas*, 21(11):110501, 2014.

[29] JW Hughes, D Mossessian, K Zhurovich, M DeMaria, K Jensen, and A Hubbard. Thomson scattering upgrades on alcator c-mod. *Review of scientific instruments*, 74(3):1667–1670, 2003.

[30] NP Basse, A Dominguez, EM Edlund, CL Fiore, RS Granetz, AE Hubbard, JW Hughes, IH Hutchinson, JH Irby, B LaBombard, et al. Diagnostic systems on alcator c-mod. *Fusion Science and Technology*, 51(3):476–507, 2007.

[31] ML Reinke, YA Podpaly, M Bitter, IH Hutchinson, JE Rice, L Delgado-Aparicio, C Gao, M Greenwald, K Hill, NT Howard, et al. X-ray imaging crystal spectroscopy for use in plasma transport research. *Review of Scientific Instruments*, 83(11):113504, 2012.

[32] LL Lao, JR Ferron, RJ Groebner, W Howl, H St John, EJ Strait, and TS Taylor. Equilibrium analysis of current profiles in tokamaks. *Nuclear Fusion*, 30(6):1035, 1990.

[33] M Greenwald et al. Overview of experimental results and code validation activities at alcator C-Mod. *Nuclear Fusion*, 53:104004, 2013.

[34] Alexei Pankin, Douglas McCune, Robert Andre, Glenn Bateman, and Arnold Kritz. The tokamak monte carlo fast ion module nubeam in the national transport code collaboration library. *Computer Physics Communications*, 159(3):157–184, 2004.

[35] Marco Brambilla. Numerical simulation of ion cyclotron waves in tokamak plasmas. *Plasma Physics and Controlled Fusion*, 41(1):1, 1999.

[36] P. T. BONOLI, R. PARKER, S. J. WUKITCH, Y. LIN, M. PORKOLAB, J. C. WRIGHT, E. EDLUND, T. GRAVES, L. LIN, J. LIPTAC, A. PARISOT, A. E. SCHMIDT, V. TANG, W. BECK, R. CHILDS, M. GRIMES, D. GWINN, D. JOHNSON, J. IRBY, A. KANOJIA, P. KOERT, S. MARAZITA, E. MARMAR, D. TERRY, R. VIEIRA, G. WALLACE, J. ZAKS, S. BERNABEI, C. BRUNKHORSE, R. ELLIS, E. FREDD, N. GREENOUGH, J. HOSEA, C. C. KUNG, G. D. LOESSER, J. RUSHINSKI, G. SCHILLING, C. K. PHILLIPS, , J. R. WILSON, R. W. HARVEY, C. L. FIORE, R. GRANETZ, M. GREENWALD, A. E. HUBBARD, I. H. HUTCHINSON, B. LaBOMBARD, B. LIPSCHULTZ, J. RICE, J. A. SNIPES, J. TERRY, S. M. WOLFE, and ALCATOR C-MOD TEAM. Wave-particle studies in the ion cyclotron and lower hybrid ranges of frequencies in alcator c-mod. *Fusion Science and Technology*, 51:401–436, 2007.

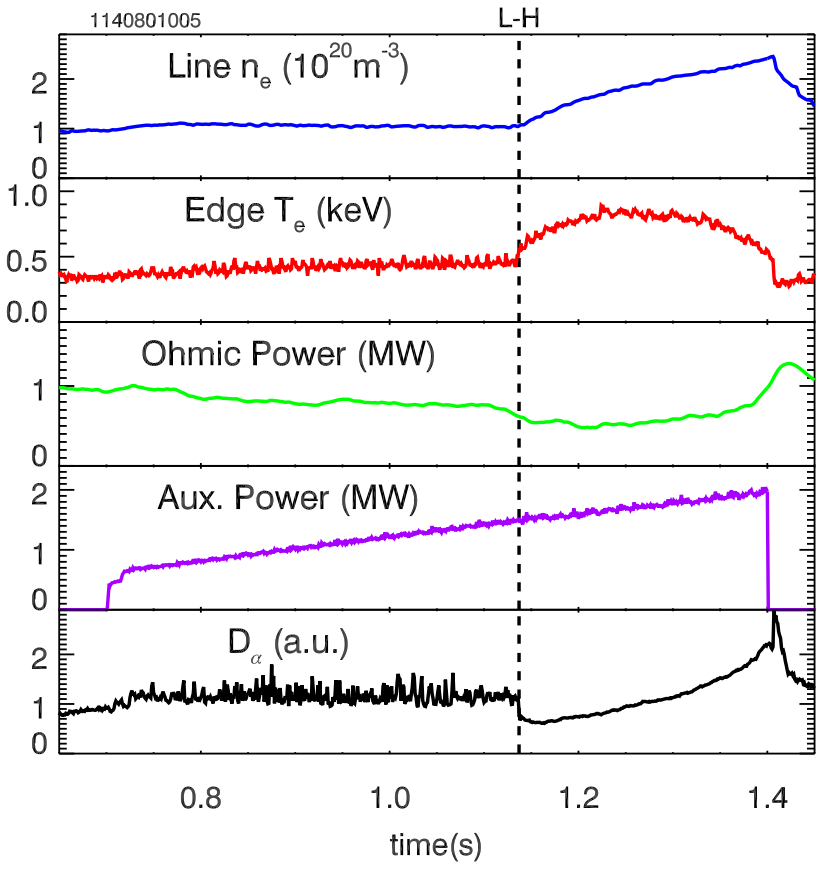

Figure 1: Time traces of selected quantities, for discharge 1140801005. From top to bottom: line-average density, electron temperature from ECE at $r/a \approx 0.86$, ohmic power, auxiliary RF power, visible D_α emission.

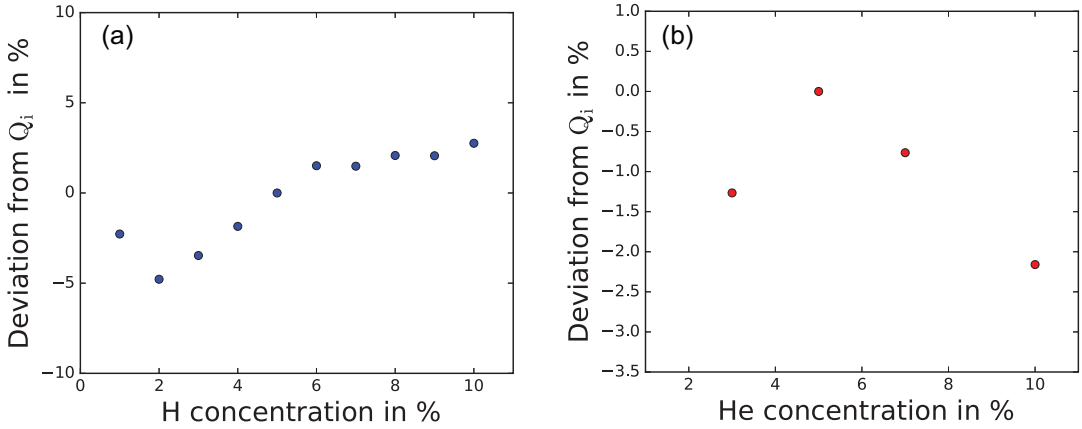

Figure 2: Sensitivity of calculated Q_i on (a) hydrogen minority concentration for D(H) ICH on C-Mod discharge 1140801032 and (b) helium-3 minority concentration for D(^{3}He) ICH on discharge 1160713011.

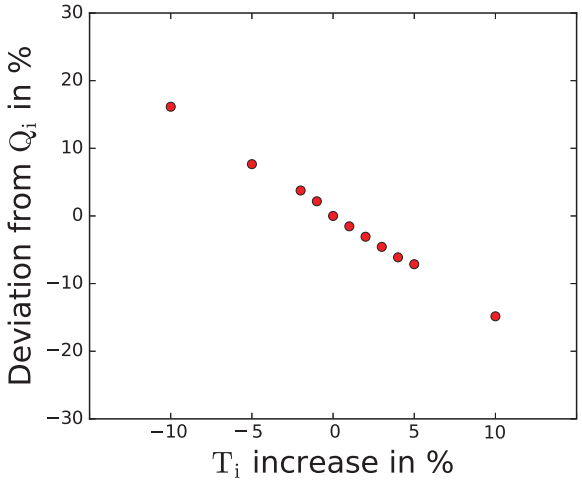

Figure 3: Deviation from baseline $Q_{i,edge}$ with varying T_i for discharge 1140801032.

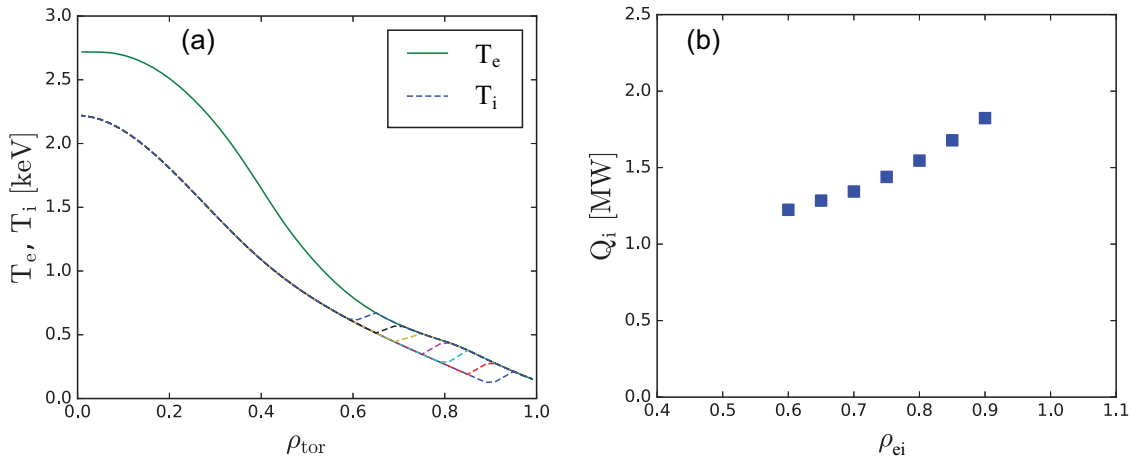

Figure 4: Calculation of Q_i for discharge number 1160713011 at 7.8T; (a) Ion and electron temperature profiles used in a series of TRANSP calculations. Outside a chosen ρ_{ei}, T_i is set equal to T_e. (b) Impact of different ρ_{ei} on Q_i.

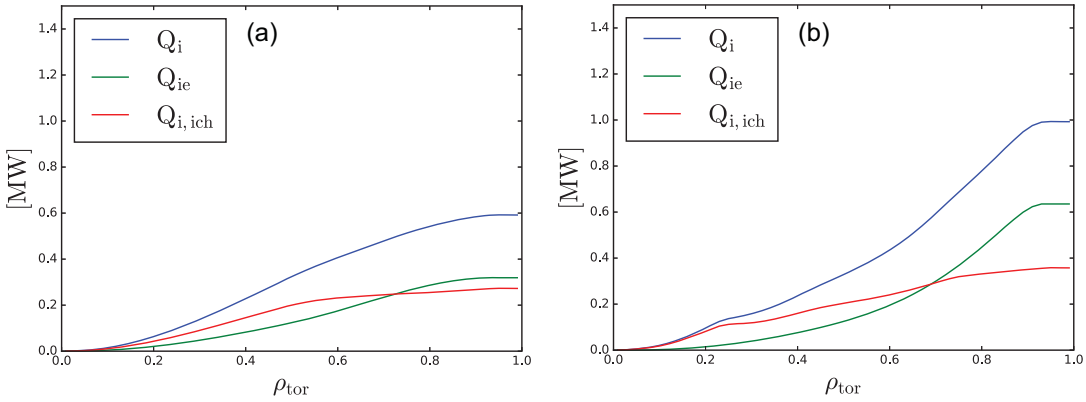

Figure 5: Profiles of the surface integrated heat flux (Q_i), as well as its components ($Q_{i,ICH}$ and Q_{ie}) at the L-H transition for discharges (a) 1150804021 ($\bar{n}_e = 0.94\ 10^{20} m^{-3}$) and (b) 1150804009 ($\bar{n}_e = 1.36\ 10^{20} m^{-3}$). Both discharges have $B_T = 5.4T$ and $I_P = 0.9MA$.

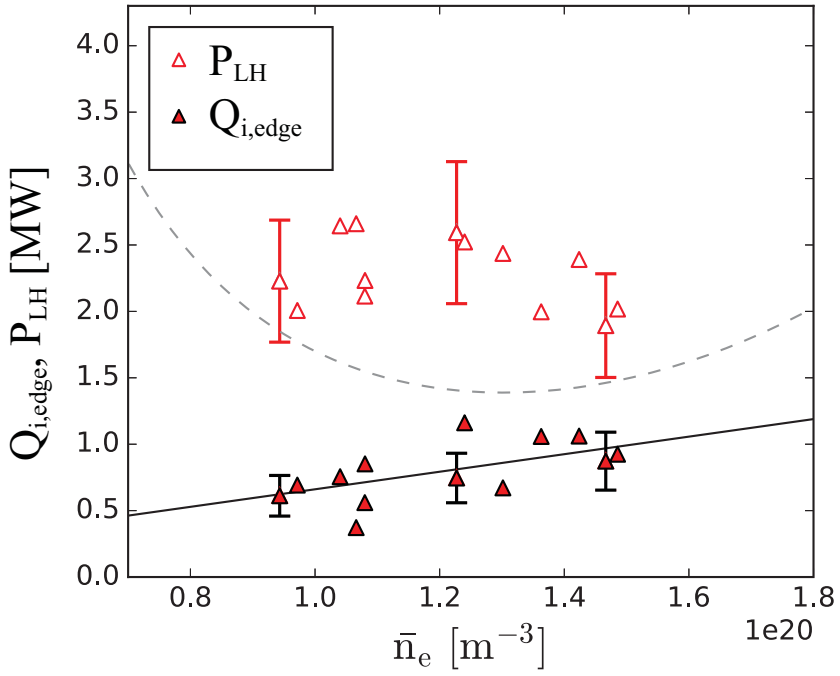

Figure 6: $Q_{i,edge}$ and P_{LH} versus density $\bar{n}_e$ just before the L-H-transition with $B_T = 5.4T$ and $I_P = 0.9MA$. The solid black line is the fit through the $Q_{i,edge}$ points which was forced through the origin. The dashed curve represents the fit to P_{LH} from [1].

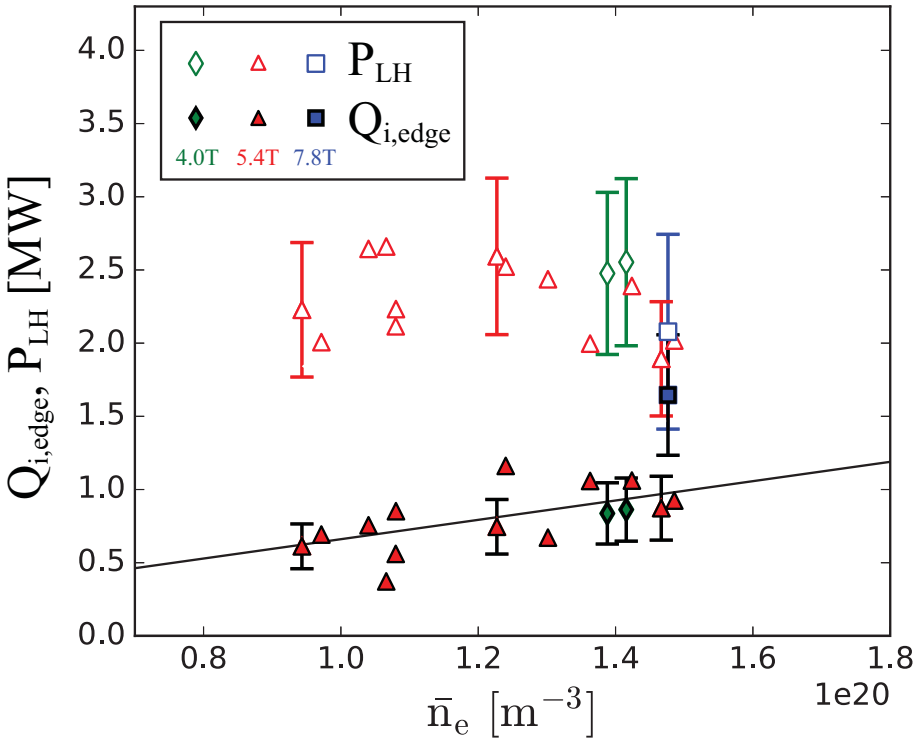

Figure 7: $Q_{i,edge}$ and P_{LH} versus density $\bar{n}_e$ in just before the L-H-transition. The solid blue square represents a discharge with B_T =7.8T and lies significantly above the 5.4T points in red. The green diamonds represent cases with 4T. The black line reproduces the a fit through the 5.4T cases as shown in Figure 6.

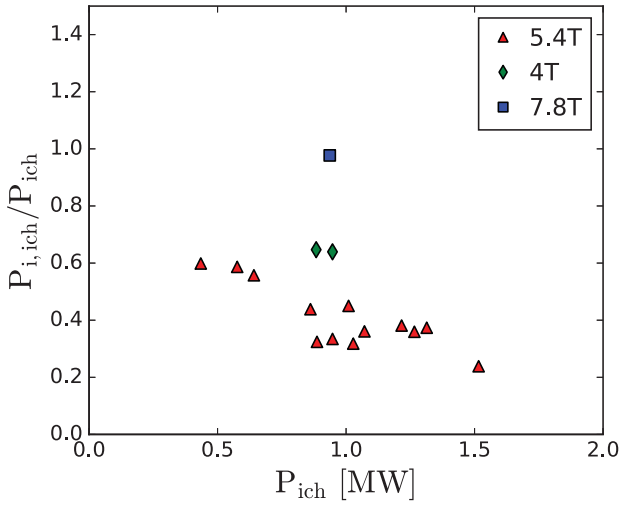

Figure 8: Ratio of direct ICH ion heating to total ICH power, versus total ICH power.

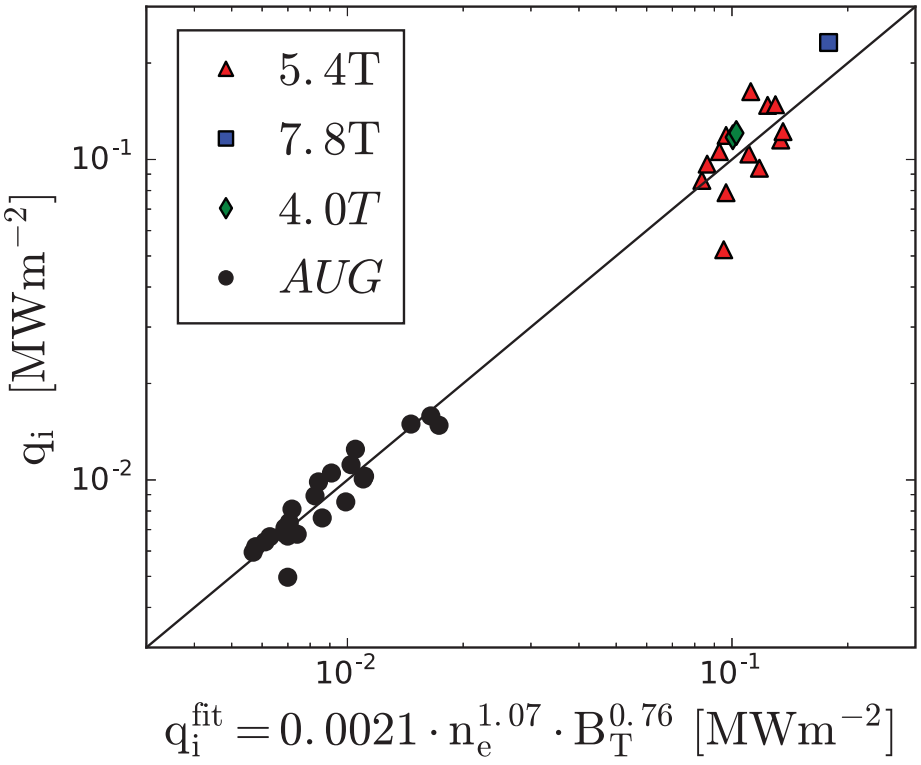

Figure 9: Experimental $q_{i,edge}^{LH}$ versus $q_{i,fit}^{LH}$ for ASDEX Upgrade and Alcator C-Mod.